

Dielectric relaxation properties of carboxylic acid-terminated n-alkyl monolayers tethered to Si(1 1 1): dynamics of dipoles and gauche defects

Christian Godet

▶ **To cite this version:**

Christian Godet. Dielectric relaxation properties of carboxylic acid-terminated n-alkyl monolayers tethered to Si(1 1 1): dynamics of dipoles and gauche defects. Journal of Physics: Condensed Matter, 2016, 28 (9), pp.094012. 10.1088/0953-8984/28/9/094012 . hal-01301355

HAL Id: hal-01301355

https://univ-rennes.hal.science/hal-01301355

Submitted on 22 Apr 2016

HAL is a multi-disciplinary open access archive for the deposit and dissemination of scientific research documents, whether they are published or not. The documents may come from teaching and research institutions in France or abroad, or from public or private research centers.

L'archive ouverte pluridisciplinaire **HAL**, est destinée au dépôt et à la diffusion de documents scientifiques de niveau recherche, publiés ou non, émanant des établissements d'enseignement et de recherche français ou étrangers, des laboratoires publics ou privés.

Published in the *Journal of Physics: Condensed Matter*

Special issue :

"**Molecular functionalization of surfaces for device applications** ",

Dielectric relaxation properties of carboxylic acid-terminated *n*-alkyl monolayers tethered to Si(111) : dynamics of dipoles and gauche defects.

C Godet

Institut de Physique de Rennes, UMR 6251 CNRS - Université de Rennes 1,

35042 Rennes Cedex, France

Email: christian.godet@univ-rennes1.fr

Abstract

Molecular-level insights into the organization and dynamics of *n*-alkyl monolayers covalently bonded to Si(111) were gained from admittance measurements of dipolar relaxation in rectifying Hg // HOOC-$C_{10}H_{25}$ – *n* Si junctions performed as a function of applied voltage and temperature. A collective behavior of dipole dynamics is inferred from the non-Debye asymmetric relaxation peak shape and strong coupling of the dipole relaxation path with some bending vibrations of the *n*-alkyl OML (multi-excitation entropy model). A variety of relaxation mechanisms is observed in the frequency range (0.1 Hz - 10 MHz) with different dependence of relaxation frequency and dipolar strength on measurement temperature and applied voltage. Their microscopic origin is discussed by comparing the activation energy of relaxation frequency with previous molecular mechanics calculations of saddle point energy barriers for structural defects such as gauche conformations or chain kinks in *n*-alkanes assemblies. Gauche conformations organized in pairs (kinks) have vanishing relaxation strength below an order-disorder transition temperature T_D = 175 K and their probability strongly increases with applied reverse voltage, above T_D. The presence of hydrogen bonds between terminal carboxylic acid functionalities is inferred from a comparison with a similar junction bearing a low density of carboxylic acid end groups. This temperature-dependent hydrogen-bond network provides some additional stiffness against external electrostatic stress, as deduced from the rather weak sensitivity of relaxation frequencies to applied bias voltage.

Keywords:

admittance spectroscopy ; dipolar relaxation ;

gauche defect ; kink ;

organic monolayer ; carboxylic

1. Introduction

While self-assembled organic monolayers (OML) form dense quasi two-dimensional sheets of oriented molecular moieties, interacting laterally through van der Waals forces, covalent tethering to crystalline semiconductor (SC) surfaces establishes additional periodic constraints at molecular heads which influence topological order and may lead to some transverse gradient of disorder [**1, 2**]. Molecular conformation of these soft layers is obviously sensitive to immobilization methods and resulting OML characteristics, e.g. molecular packing density, dipole-dipole interactions, interactions between tail-group functionalities … but possibly also to external parameters, e.g. temperature, applied pressure, selective adsorption of molecular or bio-molecular species, solvent effects.

In the field of molecular electronics, a wide range of device scales has been used to investigate electrical transport **[3]** from single molecule (conducting AFM, STM, break junctions) to large area junctions using either liquid Hg drop or solid evaporated metal as the top electrode. Robust junctions are obtained by direct binding of molecular monolayers to hydrogenated Si(111) surfaces through Si-C covalent bonds and such metal / organic monolayer / semiconductor hetero-structures have often been considered as benchmark devices to understand charge carrier transport through saturated (e.g. *n*-alkyl) or unsaturated (e.g. aromatic) molecules **[4-7].** However, despite strong experimental and simulation efforts, it is not yet clear how local or average molecular configurations affect the electronic properties of molecular layer / silicon assemblies, e.g. electronic band alignment, energy barriers for thermionic emission or tunneling of charge carriers.

Different structural and conformational models have been proposed to analyze electron transport properties of grafted molecular monolayers **[8-12]**. In *n*-alkyl – Si assemblies, shorter tethered polyethylene $(CH_2)_n$ chains ($n < 14$) are more sensitive to global tilting of the average backbone orientation upon application of some small electrostatic pressure (electrostriction effect) **[8]** and temperature-induced disorder decreases the average chain-tilting **[11].** It has been concluded that end gauche defects, i.e. non planar $(CH_2)_n$ chain conformations located at the molecular tail, do not play a dominant role for transport through OML junctions **[9]** but little information is available on the effect of other topological defects. The energetics of *gauche* bonds in OML systems is a complex matter. Experimental studies and molecular dynamics simulations have emphasized the essentially all *trans* chain conformation of the *n*-alkyl backbone in the ordered phase at low temperature and the increasing probability of gauche defects as temperature increases in the range 200-400 K **[13-17]**. However, in densely-packed *n*-alkyl monolayers, apart from terminal *gauche* bonds at chain tails, the simplest conformational sequence which approximately maintains the overall chain orientation is probably a pair of *gauche* bonds forming a "kink" in an otherwise all *trans* chain **[18].**

In order to elucidate the nature of conformational defects and their potential role in electrical transport properties in real molecular junctions, e.g. with applied voltage bias at variable temperature,

broadband admittance spectroscopy measurements can readily be performed using a well-defined metal – OML – SC planar configuration relevant for molecular electronics devices **[7, 12, 19-22]**. A proper choice of the SC doping type allows achievement of rectifying metal // *n*-alkyl – Si junctions which provides extremely low conductance (G) and small response frequency of the space-charge layer (SCL) $f_{SCL} = (G / 2\pi C)$ in the reverse voltage regime, ideally below 1 Hz at ambient temperature **[7].** At higher frequencies, the measured device admittance results either from modulation of localized electrical charge density (e.g. electron traps at the Si surface) ot from the ability of molecular dipoles to reorient in response to a time-dependent electric field **[23, 24]**. In *n*-alkl monolayers, the dipole moment of non-centrosymmetric methylene conformations will depend on details of the trans-gauche sequences while their dynamic properties (relaxation frequency and related activation energy) are expected to be affected by sterical constraints related to OML structure and chain conformation. Molecular-level insights into the dynamics of defect reorientation is also important to identify various channels of energy dissipation which govern tribological properties of functionalized surfaces **[25-27]**.

In previous studies, peak shape analysis has revealed a non-Debye behavior of dipolar relaxation, due to many-body interactions, interpreted as collective dynamic behavior of *n*-alkyl chains tethered to Si(111) **[21, 22**]. The strong decrease in relaxation frequency values with increasing reverse voltage has revealed additional motional constraints; the simultaneous increase of their activation energies was attributed to electrostatic pressure applied to the nanometer-thick monolayer **[22]**. Finally, to account for the observed correlation between activation energy and logarithm of pre-exponential factor, a multi-excitation entropy model has been proposed, where the molecular reorientation path is strongly coupled with a large number of low energy excitations (here *n*-alkyl bending vibrational mode) collected from the thermal bath **[22]**.

In this work, to obtain new insights in the organization of soft tethered monolayers at the molecular level, admittance measurements of dipolar relaxation in rectifying Hg // HOOC-$C_{10}H_{25}$ – *n* Si junctions have been performed as a function of applied bias voltage and temperature. As compared with a previous study **[22]** using a low density of carboxylic acid functionality at molecular tails (referred to as the **Si-Acid 5** junction) and slightly larger overall coverage, this molecular junction (**Si-Acid 100** junction) shows a weaker decrease in relaxation frequency with increasing reverse voltage and it allows a more comprehensive investigation of both relaxation frequency and effective dipolar strength, over a broader range of V_{DC} values. A complex behavior characterized by a large number of relaxation peaks is observed in the available frequency range (0.1 Hz - 10 MHz), requiring particular care in spectral decomposition of the frequency response; possible microscopic origin for each relaxation mechanism is discussed on the basis of their activation energy, their sensitivity to applied voltage and previous dynamic studies of structural defects such as gauche conformations or chain kinks in either free or tethered *n*-alkane assemblies.

2. Experimental

Covalent binding of *n*-alkyl monolayers to Si(111) surfaces was performed using a UV-assisted liquid-phase process to obtain well-defined and robust molecular assemblies (**section 2.1**). Molecular coverage and monolayer thickness were derived from X-ray photoelectron spectroscopy (XPS) (**section 2.2**). Current-voltage and admittance characteristics were measured over a broad temperature and applied reverse voltage range to investigate dipolar relaxation activation energy and dipolar strength values (**section 2.3**).

2.1 Covalent immobilization of acid-functionalized OML

Carboxylic acid-terminated alkyl monolayers were prepared on hydrogen-terminated Si(111):H via direct photochemical hydrosilylation of undecylenic acid, as described previously **[28].** This UV-assisted process provides covalent immobilization of well-defined dense monolayers on the oxide-free Si surface **[29-31]**. A low-doped *n*-type Si substrate (P doped, 1-10 Ω.cm, Siltronix) was chosen to obtain rectifying junctions. After etching in NH_4F, the Si(111):H surface was used immediately for covalent binding of the *n*-undecanoic acid-terminated monolayer (denoted as **Si-Acid 100**), using the photochemical reaction at 300 nm for 3 h of Si(111):H with neat undecylenic acid. The carboxylic acid-modified surface was rinsed copiously with acetone, then dipped in hot acetic acid and dried under an argon stream **[31]**.

2.2 XPS analysis

XPS measurements were performed with a Mg $K\alpha$ ($h\nu$ = 1253.6 eV) X-ray source, at normal emission angle (α = 0°), using an Omicron HA100 electron energy hemispherical analyser at 22 eV pass energy (overall resolution of 1.0 eV). Spectral analysis includes Shirley background subtraction and peak separation using mixed Gaussian-Lorentzian functions. Assuming a homogeneous organic layer on top of the Si substrate, the thickness d_{OL} is derived from the angular averaged signal $[\text{Si 2p}]_{OML} / [\text{Si 2p}]_{BARE} = \exp(-d_{OL} / \lambda_{OL} \cos \alpha)$ using the inelastic mean free path of Si 2p photoelectrons through a dense organic layer λ_{OL} = 3.6 nm **[32, 33]**. Determination of the molecular coverage Σ_{COOH} was performed by normalizing the non-attenuated C1s signal of (HO-C=O) groups (binding energy 290.1 eV) to the Si 2p intensity of one non attenuated Si(111) plane, using the number, N_S = $7.8\times10^{14}\text{cm}^{-2}$, of atoms per unit Si(111) surface.

2.3 Admittance measurements

The sample was mounted in a Teflon cell **[7]** inside a cryostat under dry nitrogen gas flow to avoid extensive water condensation and to minimize Si oxidation during electrical measurements. Ohmic back contact was obtained by applying a silver paste electrode on the scratched Si backside and a mercury top electrode (99.999 % Fluka, contact area $S = 5\times10^{-3}$ cm^2) was used to avoid electrical shorts through possible pinholes in the OML. Current (I) - voltage (V) characteristics measured using a Keithley 6487 picoammeter do not show abrupt changes near the Hg electrode melting temperature (T = 234 K).

Admittance measurements were performed with a frequency response analyzer (Alpha-A, Novocontrol) using a two terminal active cell with impedance converter mounted directly above the sample. The ac modulation amplitude V_{AC} was set at 20 mV, and the complex admittance is given by $Y(\omega) = (\tilde{\imath}_{AC} / \tilde{\upsilon}_{AC})$. The measured complex admittance, $Y^*(V_{DC}, T, \omega) = G_m + j\omega C_m$ may also be analyzed using the complex electrical modulus $M^* = (\varepsilon^*)^{-1} = j\omega C_0 / Y^*$ (here $C_0 = C^* / \varepsilon^*$ is arbitrarily set at 100 pF). The capacitance (4.5 pF) of the empty Teflon cell in parallel with the molecular junction was subtracted to obtain C_m. At high frequencies, useful information on dipolar mechanisms is limited by the series resistance R_S (due to bulk Si and back contact resistance).

Electrical measurements were performed after XPS analysis and further storage of the OML-Si assembly under UHV for one month. Prior to admittance measurements, reproducibility of I - V characteristics was checked at several sample locations (293 K to 173 K). Acquisition of dipolar relaxation data was performed with decreasing temperature steps (for typically one hour, stability 0.1 K) and, at each temperature, the direct current (dc) voltage was scanned from the reverse regime (V_{DC} = -2 V) towards the forward regime (V_{DC} = +1 V).

Under experimental conditions including a large electric field over the nanometer-thick monolayer, reversibility of bias voltage- and temperature-induced junction modifications can be assessed from the reproducibility of room-temperature admittance before and after the entire low temperature scan. For this Hg // HOOC-$C_{10}H_{25}$ – n Si junction, weak spectral changes were observed upon return to room-temperature (293 K), e.g. at -0.2 V the space charge layer relaxation peak remains located near 2 Hz, while the B2 peak is shifted to higher frequency by a factor of 2 while the peak strength $\Delta\varepsilon$ (B2) has increased by about 25%. Qualitatively similar effects were reported previously for the **Si-Acid 5** junction [**22**].

3. Experimental results

The C1s and Si2p signal intensities and hence the number of molecular chains grafted to the oxide-free Si(111) surface remains stable over several days in UHV. The density of acid end groups obtained by XPS provides the surface coverage (Σ_{COOH} = 2.0×10^{14} cm^{-2}). A consistent but slightly larger coverage (Σ_{C1s} = 2.2×10^{14} cm^{-2}) is obtained from the total C1s signal (see Supplementary information). Hence, the molecular coverage is not very high, with typically 28% of the Si(111) surface atoms being used as anchoring sites. The OML thickness (d_{OL} = 1.0±0.1 nm) indicates formation of an alkyl monolayer with rather large average tilt angle (55°) of the chain backbone with respect to the normal direction. Si 2p spectra at large emission angles (α = 45°) show no trace of Si oxidation.

As expected for metal // *n*-alkyl – Si junctions using *n*-type silicon [**7, 9, 28]**, strong rectification is obtained in the current-voltage characteristics of Hg // HOOC-$C_{10}H_{25}$ – *n* Si junctions (**Figure 1**). Analysis of *I* (*V*, *T*) characteristics was performed by considering a Schottky barrier in series with a tunnel barrier, according to a procedure described previously **[7]**. In the low forward voltage regime (0.05–0.35 V), it provides the junction ideality factor (*n* = 1.68±0.03) and a *T*-dependent effective barrier height, $q\Phi_{EFF}(T) = q\Phi_B + (kT)\beta^0 d_T$, which results from the band bending in the semiconductor (space-charge layer) and from the effective attenuation of the OML tunnel barrier, $\exp(-\beta^0 d_T)$, where $\beta^0 = 2\left(2m^*\Phi_T/\hbar^2\right)^{\frac{1}{2}}$ is the inverse attenuation length at zero applied voltage, $\hbar$ the reduced Planck's constant and *m** the effective mass of electrical carriers in the OML. The y-axis intercept of $\Phi_{EFF}(T)$ is the semiconductor barrier height, $q\Phi_B^J \approx 0.62\pm0.02$ eV and the slope gives the tunnel attenuation factor, $\beta^0 d_T = 8.9 \pm 0.7$, of the junction. Using d_T = 1.0 nm, the resulting inverse attenuation length, β^0 = 0.9 Å^{-1} is similar to that observed in other *n*-alkyl junctions **[3, 7]**.

These results as a whole show that the structure and electrical properties of the Hg // HOOC-$C_{10}H_{25}$ – *n* Si junction are quite similar to previous metal-OML-Si devices reported in the literature. In the following, guidelines are given to discriminate dipolar relaxation against space-charge layer response (**Section 3.1**) and to obtain the characteristic peak shape of each dipolar relaxation mechanism (**Section 3.2**). The frequency and dipolar strength values resulting from data analysis will be described as a function of temperature (**Section 3.3**) and reverse dc voltage (**Section 3.4**).

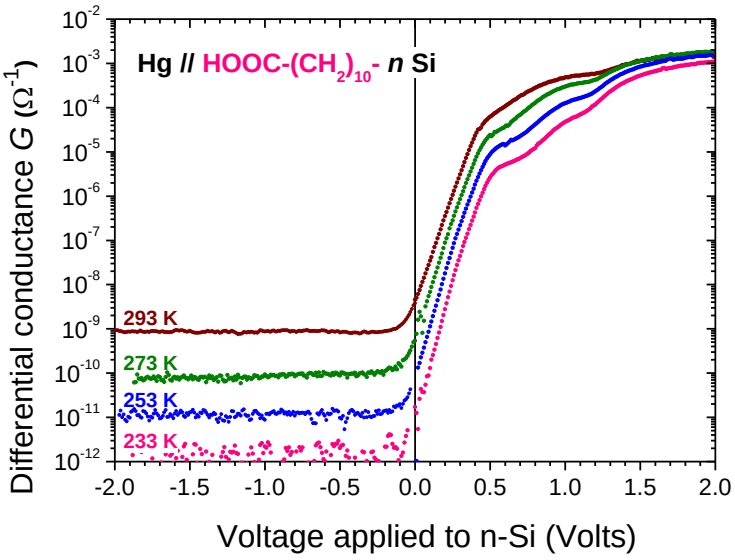


Figure 1 : Differential conductance (*G*) obtained by numerical derivation of *I* - *V* characteristics of the Hg // Acid 100 – *n*-Si junction.

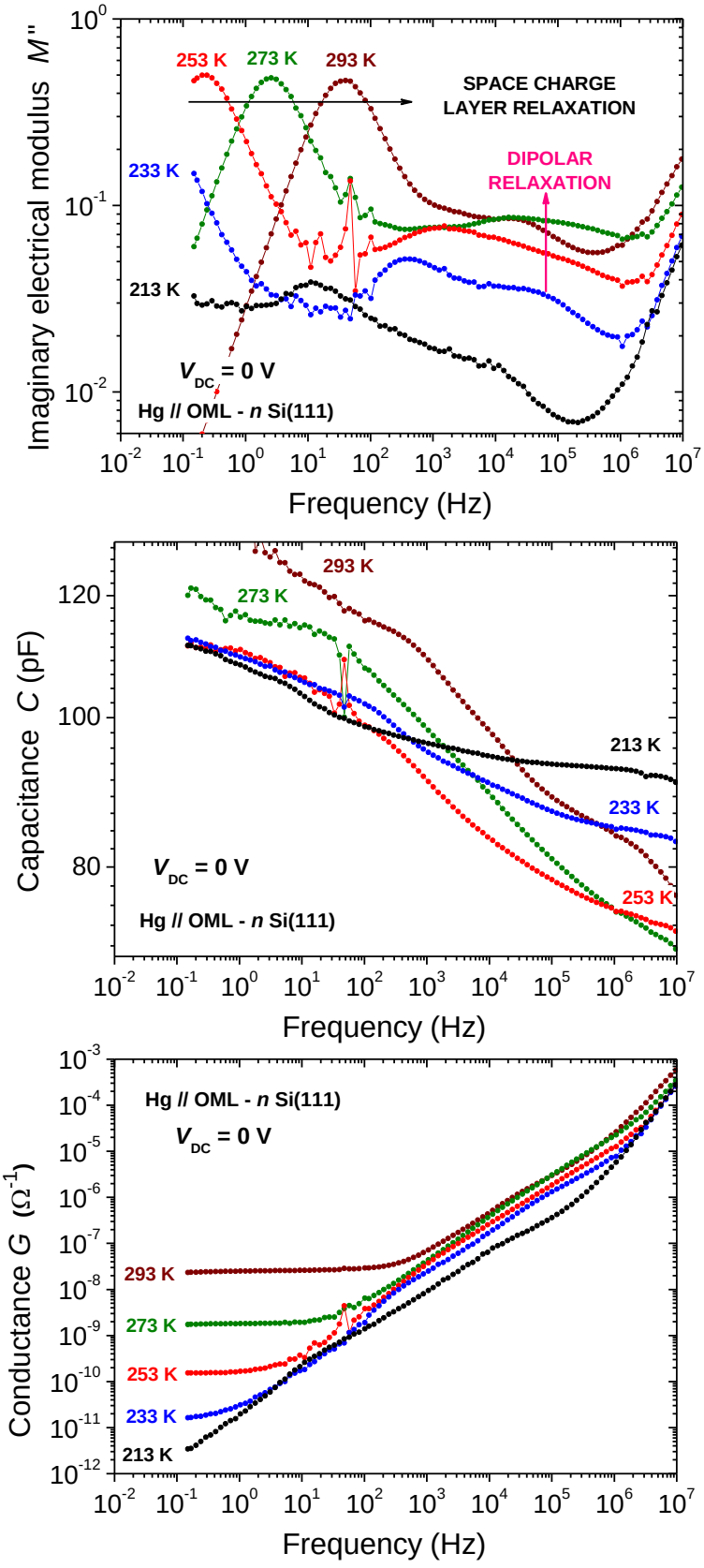


Figure 2 Temperature dependence of the admittance of the Hg // Acid 100 – Si junction (V_{DC} = 0 V): a) imaginary electrical modulus $M''(\omega)$; b) capacitance $C(\omega)$; c) real admittance $G(\omega)$. A clear discrimination between space-charge layer and OML dipolar relaxations appears in the electrical modulus representation. A larger noise level can be found at the grid frequency (50 Hz).

3.1 Space-charge layer response vs dipolar relaxation

Figure 1 shows the differential conductance obtained by numerical derivation of *I* - *V* characteristics, between 233 and 293 K. Within a factor of two, differential conductance values match the real part of the admittance $Y(\omega)$ plateau obtained in the low frequency limit (**Figure 2.c**). Since the capacitance $C(\omega)$ remains close to 100 pF for all temperatures (**Figure 2.b**), the response frequency of the space-charge layer $f_{SCL} = (G / 2\pi C)$ essentially follows the conductance variations, e.g. at 273 K, $G(\omega) = 1.5\times10^{-9}\ \Omega^{-1}$ at low frequency and the imaginary electrical modulus *M*" shows a strong peak at $f_{SCL} = (G / 2\pi C) \approx 3$ Hz (**Figure 2.a,** $V_{DC} = 0$ V).

For V_{DC} values in the forward voltage range, the space charge layer response appears in the measurement frequency window (0.1 Hz – 10 MHz); at $V_{DC} = 0$ V, the SCL response is still visible at 233 K, hence lower temperatures ($T \leq 213$ K) are required to remove the SCL contribution from the acquisition range (**Figure 2.a**).

In addition to the relaxation frequency behavior, the electrical modulus $M''(\omega)$ representation of admittance data provides a clear criterion to discriminate the broad asymmetric relaxation mechanisms related to the OML dipolar response, defined by apparent pre-peak slope ($m_{DH} < 1$) and post-peak slope ($1\text{-}n_{DH} < 1$), and the symmetrical SCL peak shape ($m_{SCL} = 1$, $n_{SCL} = 0$).

3.2 Dipolar relaxation: peak shape analysis

Figure 3 shows several representative plots of the imaginary electrical modulus *M"* vs frequency (log - log scale), where five peaks are easily identified and denoted as B0, B1, B2, C, D in the order of increasing frequency values at a given temperature. In our measurement conditions, no other relaxation peak is detected in the frequency window 0.1 Hz – 100 kHz.

For each relaxation mechanism, four parameters ($\Delta\varepsilon$, ω_{DH}, m_{DH}, n_{DH}) are necessary to describe the complex dielectric permittivity in the framework of Dissado-Hill theory for many-body interactions in complex systems **[21, 22 34, 35]**:

$$\varepsilon(\omega) - \varepsilon_\infty(\omega) = \Delta\varepsilon\,[1\text{-}j\omega/\omega_{DH}]^{-1+n_{DH}}$$

$$\times\ {}_2F_1[1\text{-}n_{DH}\ ,\ 1\text{-}m_{DH}\ ;\ 2\text{-}n_{DH}\ ;\ (1\text{-}j\omega/\omega_{DH})^{-1}]\ /\ {}_2F_1[1\text{-}n_{DH}\ ,\ 1\text{-}m_{DH}\ ;\ 2\text{-}n_{DH}\ ;\ 1] \qquad (1)$$

where ${}_2F1\ (\ ,\ ,\ ;\ ;\ )$ is the Gauss hypergeometric function with $0 \leq m_{DH} \leq 1$ and $0 \leq n_{DH} \leq 1$, ω_{DH} is the peak frequency and ω is the frequency. Since a large number of overlapping peaks often results in some underdetermined parameter fitting, pre-peak and post-peak slopes are obtained by the procedure described below, and set constant over a wide range of temperatures and V_{DC} values, while the frequencies and dipolar strengths are fitted by minimizing the error function EF($\Delta\varepsilon$,

ω_{DH}, m_{DH}, n_{DH}) given by the sum over the fitting range of [Ln (M''_{EXP} / M''_{CALC})] ^{2}. Since all peaks possibly overlap, data fitting must be performed over the whole frequency range in order to obtain accurate relaxation frequencies (f_X) and effective dipolar strengths ($\Delta\varepsilon_X$). In some conditions (e.g. large reverse voltage), a larger noise level may require additional fitting constraints.

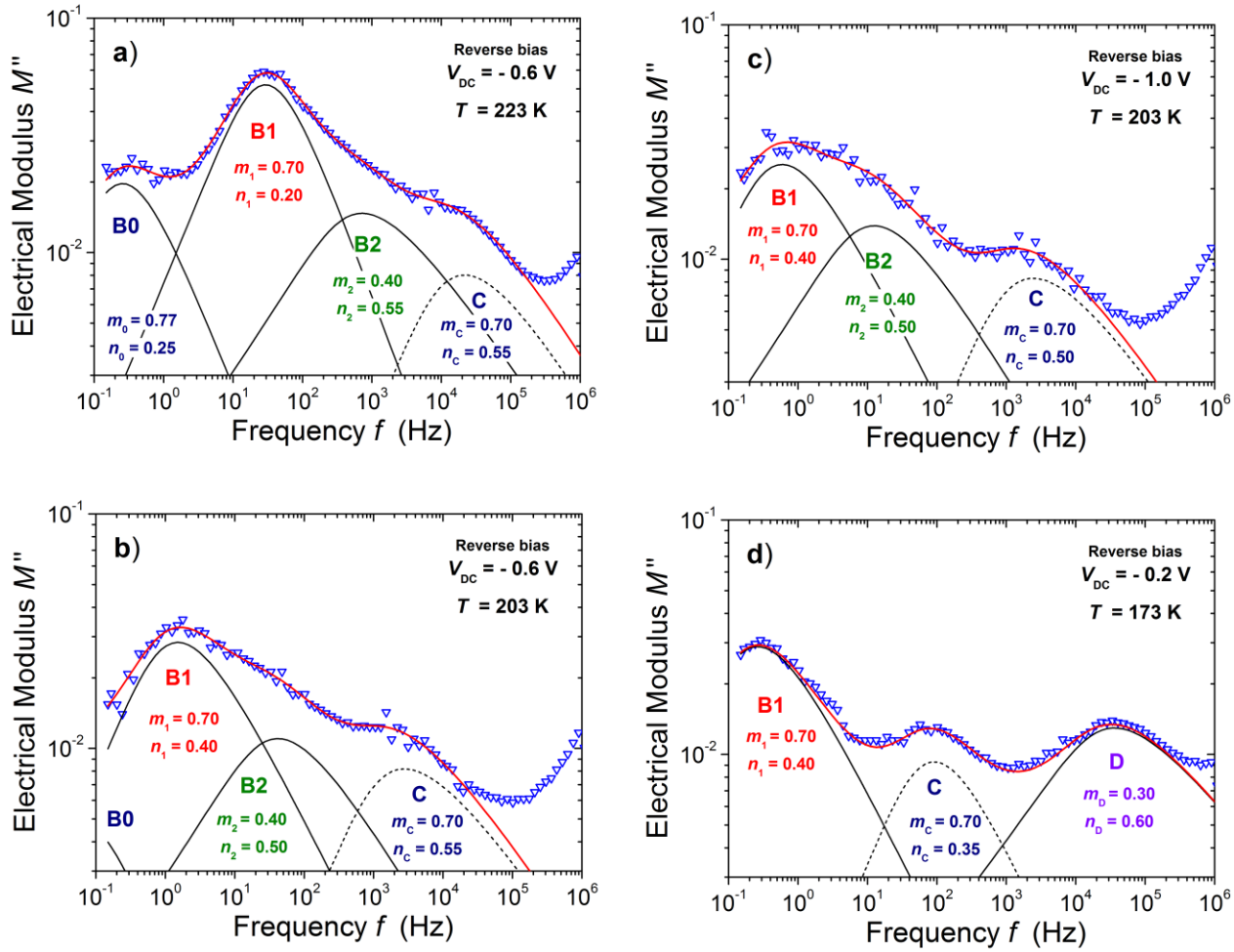


Figure 3 Determination of asymmetric peak shape parameters (Dissado-Hill theory, **Eqn 1**) for each dipolar relaxation mechanism. The red line is the peak sum fitted to data (open triangles):

a) T = 223 K, V_{DC} = -0.60 V (m_1 = 0.70, n_A = 0.55).

b) T = 203 K, V_{DC} = -0.60 V (m_1= 0.70, n_2 = 0.50, n_A = 0.55) ;

c) T = 203 K, V_{DC} = -1.0 V (m_1= 0.70, n_2 = 0.50, n_A = 0.50) ;

d) T = 173 K, V_{DC} = -0.20 V (n_1 = 0.40, m_A = 0.70, n_A = 0.35, m_C = 0.30, n_C = 0.60).

In order to impose a constant peak shape for each relaxation mechanism, we have chosen to evaluate pre-peak (m) and post-peak (n-1) slopes in some unambiguous measurement conditions, as described below. At relatively high temperature and intermediate reverse voltage (**Fig. 3.a**, T = 223 K, V_{DC} = -0.60 V), pre-peak B1 slope (m_1 = 0.70) and post-peak C slope (n_C = 0.55) are readily obtained. For all mechanisms, peak frequencies strongly decrease with decreasing measurement temperature (**Fig. 3.b**, T = 203 K, V_{DC} = -0.60 V) but pre-peak and post-peak slope values remain unaffected. The B0 peak shape has been adjusted at high temperature (T = 223 K, m_0 = 0.77, n_0 = 0.25).

A constant B1 peak shape is found for a broad T range (173 - 223 K). However, a narrower B1 peak shape (m_1 = 0.80, n_1 = 0.20) must be set for data fitting at 233 K and above, otherwise the fitted dipolar strength $\Delta\varepsilon$(B2) shows a very broad random dispersion and the fitted frequency f (B2) is no longer consistent with the activated behavior observed at $T \leq$ 223 K; interestingly, taking into account this peak narrowing effect does not change f(B1) values but it reconciles high temperature data with the temperature-independent dipolar strength $\Delta\varepsilon$(B1) found below 213 K.

With increasing reverse voltage (**Fig. 3.c**, T = 203 K, V_{DC} = -1.0 V), a decrease in frequency appears for both peaks B1 and B2, in contrast with a remarkable stability in peak C frequency. The increasing dipolar strength of peak B2 allows better determination of post-peak B2 slope (n_2 = 0.50) and consequently more accurate pre-peak C slope (m_C = 0.70). Determination of pre-peak B2 slope (m_2 = 0.40) is less obvious and any error will affect absolute values of the fitted dipolar strength. Note that slightly steeper post-peak slope (n_C = 0.35) is obtained for peak C when a high frequency D peak is adjusted above 100 kHz (**Fig. 3.d**).

At low temperatures, typically below 183 K, peak B2 virtually disappears (as illustrated in **Fig. 3.d**, T = 173 K, V_{DC} = -0.20 V) and the imaginary electrical modulus M'' at low frequencies can be fitted using peak B1 alone, providing post-peak B1 slope (n_1 = 0.40). Under this low temperature condition, relaxation frequency of peak D has decreased near 30 kHz, which allows an accurate determination of pre-peak and post-peak D slopes (m_D = 0.30, n_D = 0.60). Some narrowing of peak C is also found at 173 K (**Fig. 3.d**, m_C = 0.75, n_C = 0.35) and 153 K (**Table 1,** m_C = 0.80, n_C = 0.25), possibly indicating a modified OML structure, either in alkyl chain packing or in end group conformations, at very low temperature.

In summary, pre-peak and post-peak slope values derived from the above approach and summarized in **Table 1** are suitable to describe experimental results over a wide range of temperatures and V_{DC} values. Clear departure from the constant-shape assumption only occurs in the lower temperature range, typically T < 173 K and for the post-peak B1 slope at higher temperatures, n_1 = 0.2 for $T \geq$ 223 K (**Fig. 3.a**).

Temperature range	m_0	n_0	m_1	n_1	m_2	n_2	m_C	n_C
$T \geq 233$ K	0.77	0.25	0.80	0.20	0.40	0.50	0.70	0.55
173 K - 223 K	0.77	0.25	0.70	0.40	0.40	0.50	0.70	0.55
153 K	0.70	0.60	0.70	0.30	0.40	0.50	0.80	0.25

Table 1 : Shape analysis of the dipolar relaxation peaks: pre-peak slope (m_{DH}) and post-peak slope (n_{DH} -1) are given by **Eqn. 1**. A constant shape is found for a broad T range (173 - 223 K) while a narrowing of B1 peak shape occurs above 233 K.

3.3 Temperature dependence at low V_{DC}

Using this fixed-shape analysis procedure, a consistent behavior of relaxation peak frequencies and dipolar strength is observed, as a function of measurement temperature and applied voltage.

For relaxation mechanisms B2 and C, above 180 K, relaxation peak frequencies follow a clear Arrhenius dependence on temperature, $f_X = f^0_X \exp[- E_X / kT]$, over two to three decades, as illustrated in **Fig.4a** (V_{DC} = -0.10 V). At low applied voltage (-0.2 V $\leq V_{DC} \leq$ 0 V), nearly constant E_X values are observed: 0.38±0.02 eV (B2) and 0.46±0.02 eV (C), corresponding to pre-exponential factors f^0(B2) = 2×10^{11} Hz and f^0(C) = 2×10^{14} Hz. As discussed in **Section 4**, the activation energy is interpreted in terms of a minimal energy barrier governed by motional constraints for dipole reorientation. In contrast to mechanisms B2 and C, an Arrhenius plot of f_{B1} shows a pronounced curvature, with some transition near T_H = 213 K; since B1 is the most intense relaxation mechanism, artifacts due to data fitting can be discarded. The weak T-dependence of f_{B1} observed at low T is parameterized using an apparent activation energy at low-T, E_{LT}(B1) ≈ 0.32±0.02 eV, while the stronger variation of f_{B1} above 213 K is parameterized using an apparent activation energy at high-T denoted E_{HT}(B1) ≈ 0.70±0.05 eV.

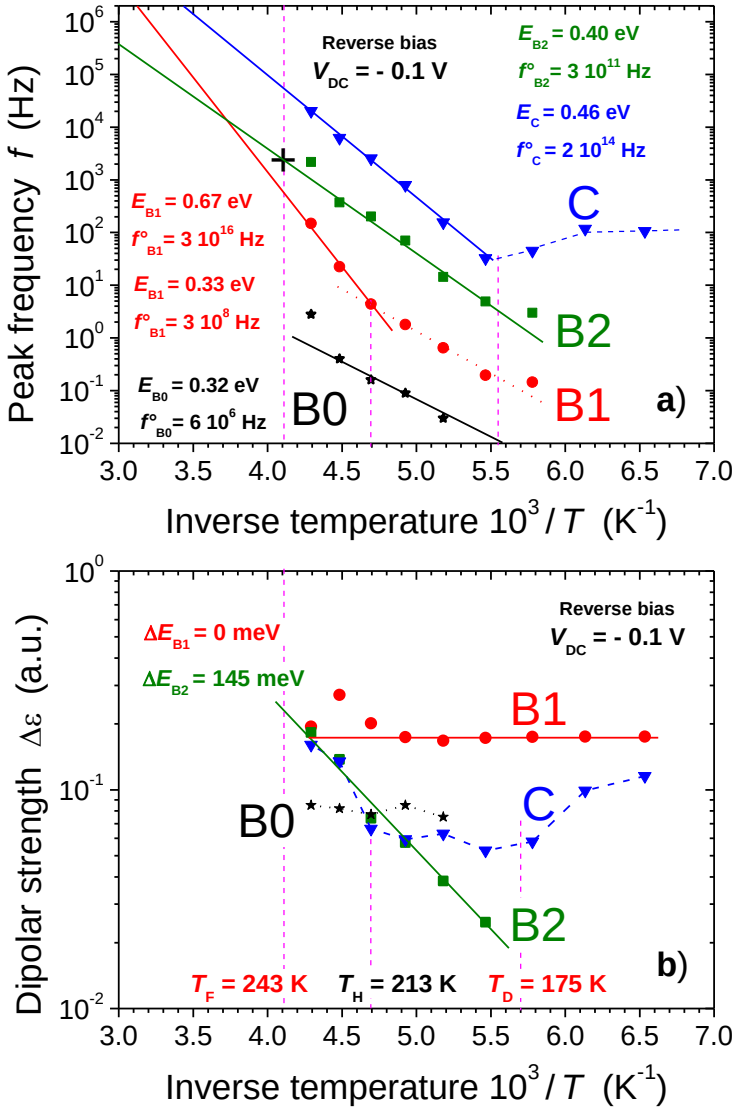


Figure 4 Temperature dependence of the dipolar relaxation frequencies f_X (a) and dielectric strength $\Delta\varepsilon$ (b) at small reverse voltage (V_{DC} = - 0.10 V) for peaks B0, B1, B2, C, D. The lines are Arrhenius fits to the frequency data in the range 183-223 K. A transition at T_H = 213 K is observed for peak B1 frequency.

Dipolar strength ($\Delta\varepsilon_X$) decreases for peaks B2 and C as temperature decreases from 233 K to 183 K (**Fig.4b,** V_{DC} = -0.05 V). In contrast, a temperature-independent dipolar strength $\Delta\varepsilon$(B1) is found if the B1 peak narrowing effect near 233 K is taken into account. Interestingly, peak B2 vanishes ($\Delta\varepsilon << 0.02$) below 183 K whereas $\Delta\varepsilon$(C) increases significantly, indicating again a different OML structure at very low temperature. In this low temperature range ($T \leq 183$ K) some fits were also performed by constraining $\Delta\varepsilon$(B1) to its constant plateau value, confirming the vanishing strength of peak B2.

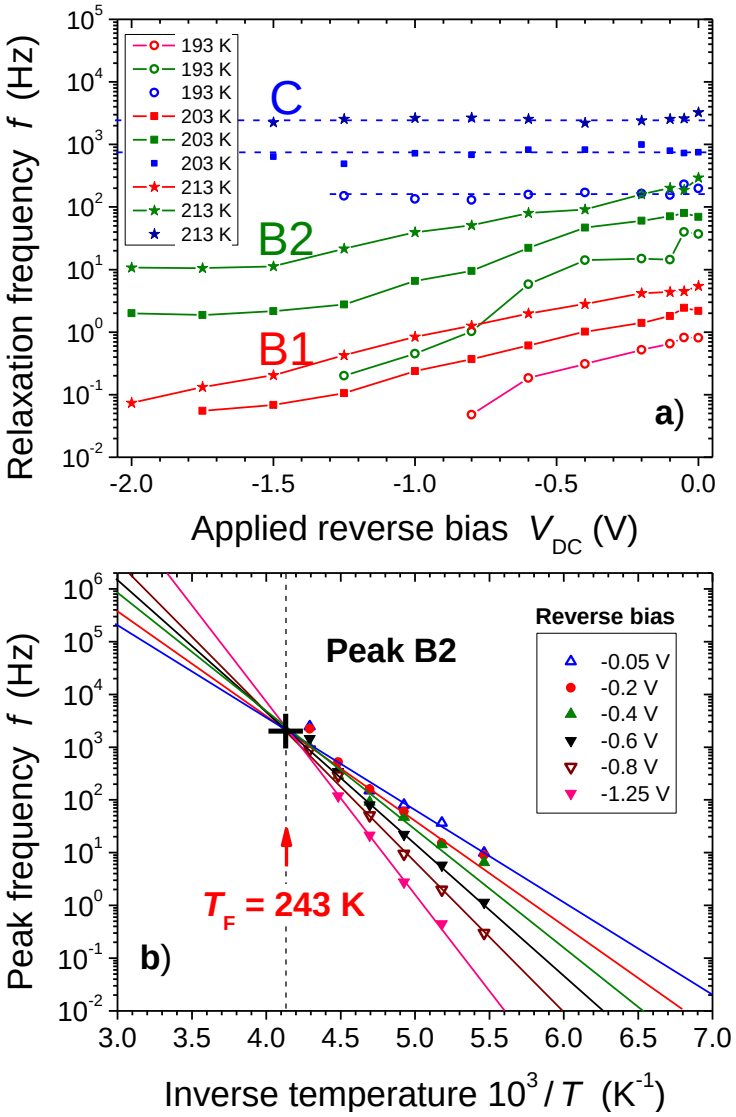


Figure 5 a) Reverse voltage dependence of relaxation frequencies for peaks B1, B2 and C at 193, 203, and 213 K. (b) Temperature dependence of f_{B2} at different reverse voltage values (V_{DC} range from -0.05 V to - 1.25 V); the lines are Arrhenius fits to the data, showing the existence of a "focal point" near T_F (B2) = 243 K.

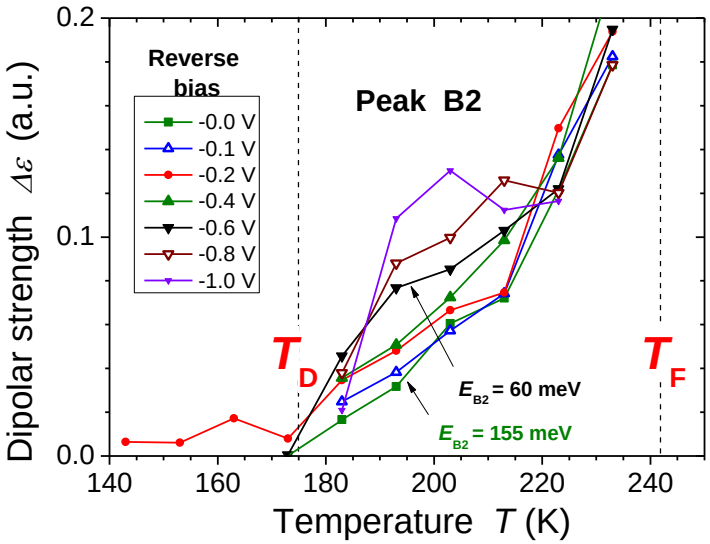


Figure 6 Dipolar relaxation strength for mechanism B2 in the Hg // Acid 100 – *n*-Si junction; $\Delta\varepsilon$(B2) increases with increasing temperature and increasing reverse voltage V_{DC} (from 0 V to - 1.0 V). The order-disorder temperature, T_D, is defined by the onset of gauche or kink defect relaxation.

3.4 Reverse bias voltage dependence of dipolar relaxation mechanisms

As illustrated in **Fig. 3**, relaxation mechanisms B1 and B2 are sensitive to the magnitude of the applied reverse voltage. A monotonous decrease of relaxation peak frequencies with increasing reverse voltage is observed, over several decades (**Fig.5a**) and the corresponding activation energy, E_X, simultaneously increases. Peak B0 basically follows the same trend but only few data are available. In contrast, a very weak effect of reverse voltage is found for peak C frequency which depends essentially on temperature with constant activation energy, $E_C \approx 0.46 \pm 0.05$ eV eV. Note that, as a consequence of poorer signal / noise ratio in *M*" data, larger error bars on fitted $\Delta\varepsilon_X$ and f_X values are obtained for stronger reverse voltage (-2.0 V $\leq V_{DC} \leq$ -0.4 V).

As far as dipolar relaxation strength is concerned, at large reverse bias, $\Delta\varepsilon_X$ decreases for peaks B2 and C as temperature decreases from 233 K to 183 K, and the temperature-independent dipolar strength $\Delta\varepsilon$(B1) is very weakly dependent on V_{DC}. The peculiar behavior of peak C below 183 K is maintained at large bias voltage applied to the Hg // Acid 100 – *n*-Si junction.

The bias voltage dependence of dipolar strength is particularly interesting for peak B2. Its monotonic decrease vs decreasing temperature (from 233 K to 183 K) is very reproducible for several low reverse voltage values, as shown in **Fig.6**. At very small reverse voltage (V_{DC} = -0.05 V), the temperature dependence of $\Delta\varepsilon$(B2) follows an Arrhenius law with activation energy of 145±10 meV. With increasing reverse voltage (-1.0 V ≤ V_{DC} ≤ -0.2 V), a significant increase of $\Delta\varepsilon$(B2) is observed, particularly in the T range 183-213 K, along with a monotonic decrease of its apparent activation energy (typically 113 meV at V_{DC} = -0.4 V, 60 meV at V_{DC} = -0.6 V and nearly zero at V_{DC} = -1.0 V). Interestingly, $\Delta\varepsilon$(B2) drops to extremely small values below T_D = 175 K, for all the investigated reverse bias voltage conditions, so that good fits of *M''* are still obtained by setting $\Delta\varepsilon$(B2) = 0 (**Fig. 3d**).

Considering the temperature-activated behavior of relaxation peak frequencies, **Fig.5b** shows that Arrhenius lines (extrapolated to high T) obtained at different V_{DC} values tend to converge at a so-called "focal point" (or isokinetic) temperature, T_F (B2) ≈ 243±5 K for mechanism B2. A slightly larger value is found for mechanism B1, T_F (B1) ≈ 250±10 K (not shown) using the frequencies obtained at high temperature (213-233 K). This result is related to the observed linear correlation between activation energy and logarithm of pre-exponential factor, shown in **Fig.7** for relaxation mechanisms B1 and B2. Similar values are obtained for the inverse slopes kT^* (C) = 19.1 meV (222 K), kT^* (B2) = 20.0 meV (232 K), kT^* (B0) = 19.3 meV (224 K) and kT^* (B1) = 20.0 meV (232 K) relevant to E_{HT}(B1) in the high temperature range. The few data available for peak D preclude any conclusion. The physical meaning of kT_F and kT^* energy values (20 meV or 161 cm^{-1} wavenumber) will be discussed in **Section 4.5,** in the context of collective relaxation dynamics.

Figure 8 displays the activation energies of the relaxation frequency as a function of applied dc voltage V_{DC} for mechanisms C (triangles), B1 (squares) and B2 (circles). The stronger sensitivity is found for peak B2, where the quadratic V_{DC} dependence E_{B2} (eV) = 0.30 + 0.55 $|V_{DC}|^2$ (**Fig. 8**, full line) at low bias is followed by some saturation at larger voltage, V_{DC} ≤ -1.0 V. A weaker increase, from 0.7 eV to 1.0 eV, is found for E_{HT}(B1). In contrast E_C remains nearly constant, within fitting error bars, over a broad V_{DC} range. For a more quantitative analysis, the increase of E_X between 0 and -1 V, denoted W(0/-1) = E_X(-1.0 V) – E_X(0 V), was obtained; their respective values, W(B2) = 0.31 eV, W(B1) = 0.23 eV, W(C) < 0.10 eV, will be discussed in **Section 4.4**.

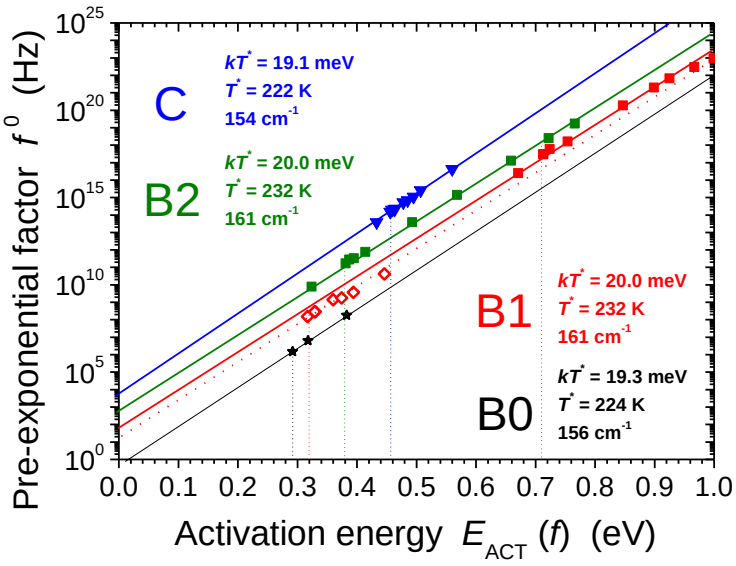


Figure 7 Linear correlation between activation energy of the relaxation frequency and logarithm of pre-exponential factor derived from **Fig.4**, for peaks B0 (stars, black), B1 (LT, diamonds, red), B1 (HT, squares, red), B2 (squares, green) and C (triangles, blue). The inverse slope is denoted kT^*.

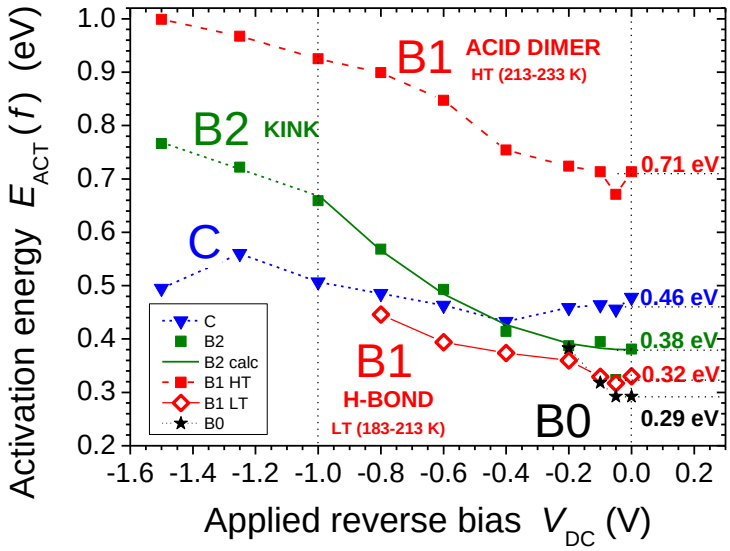


Figure 8 Activation energy of the relaxation frequency as a function of applied dc bias voltage, V_{DC}, for mechanisms B0 (stars, black), B1 (LT, diamonds, red), B1 (HT, squares, red), B2 (squares, green) and C (triangles, blue). For peak B2, the full line is a calculated power-law function with forced exponent value: $E_{B2}\,(\mathrm{eV}) = 0.38 + 0.29\ |V_{DC}|^2$.

4. Discussion

This investigation of dipolar relaxation in rectifying Hg // HOOC-$C_{10}H_{25}$ – *n* Si junctions basically confirms the main results of a previous study **[22]** on *n*-alkane OML with a low density of carboxylic acid functional groups at molecular tails (mixed acid / methyl, 5:95 ratio, denoted as **Si-Acid 5** junction). Structural characterizations based on XPS are useful for the comparison and interpretation of some differences observed in admittance experiments. The molecular coverage in the **Si-Acid 100** junction derived from the total C1s peak area (2.2×10^{14} cm^{-2}) is slightly smaller than that of the **Si-Acid 5** junction (2.6×10^{14} cm^{-2}). This result is consistent with previous studies **[31]** and with the more bulky carboxylic acid end group as compared with the methyl terminal group. Smaller molecular coverage is also qualitatively coherent with smaller thickness and larger tilt angle with respect to the normal direction found in **Si-Acid 100** (d_{SE} = 1.0±0.1 nm, $\theta \approx 55°$) vs **Si-Acid 5** (d_{SE} = 1.06±0.1 nm, $\theta \approx 40°$) derived from SE modelling. In both investigations, no trace of Si oxidation was found in the Si 2p spectra (see Supplementary Information).

However, in this study, weaker decrease in the relaxation frequency with increasing reverse bias voltage allows a more comprehensive investigation of both relaxation frequency and effective dipolar strength, over a broader range of V_{DC} and T values. The variety of relaxation mechanisms observed in this work also allows critical reconsideration of the attribution of B1 and B2 mechanisms to acid end-group dipoles and to gauche defect configurations, respectively, performed previously on the basis of voltage dependence of relaxation peak intensities **[22]**.

This discussion is built upon some concepts proposed earlier for the interpretation of admittance data: a) dipolar relaxation is a collective behaviour, where the motion of "embedded dipoles" under small bias modulation depends on spatial correlations described by the DH model **[34, 35],** b) the minimum energy required to overcome the saddle point of this dipole reorientation path is provided by elementary excitations collected from a thermal bath, as described by the multi-excitation entropy model **[22]**, c) the increased motional constraints related to the applied reverse dc bias voltage are attributed to compression and shear stresses (e.g. induced by the complex mechanical response of the soft molecular layer to electrostatic pressure, **Scheme 1** in **ref. 22**).

Molecular dynamics simulations have shown that *trans-gauche* isomerization rates in anchored bilayers are slower than in lipid bilayers at the same temperature and that they increase as the bond positions approach the tail **[36]**. Although a distribution of relaxation rates may be expected from this description, several well defined relaxation peaks and activation energies have been found in this study. The existence of several dipolar relaxation mechanisms rather than a distribution of local activation energies is further supported by the different dependence of E_X on

applied bias voltage V_{DC} (i.e. different W values). Microscopic defects such as pinholes are not considered either since they were not evidenced in scanning tunneling microscopy studies **[28]**.

4.1 Identification of dipolar relaxation mechanisms

As compared with our previous study of the **Si-Acid 5** junction **[22]**, the main novelty of this work is the large number of relaxation mechanisms observed in the experimentally available frequency window. All mechanisms (B0, B1, B2, C) show strong dependence of relaxation frequency on temperature, described by Arrhenius laws (at least above 180 K for peak C).

Three peaks (B0, $B1^{HT}$, B2) show a significant dependence of relaxation frequency on applied reverse bias voltage; this behavior is typical of mechanism "B" in our previous analysis **[22]**. Dipolar strength analysis shows that $\Delta\varepsilon$(B2) is temperature-dependent while $\Delta\varepsilon$(B1) is nearly constant below 233 K, in good agreement with the related peaks B1 and B2 observed in the **Si-Acid 5** junction **[22]**. Interestingly, the apparent activation energy of $\Delta\varepsilon$(B2) in the range 183-233 K, decreases from 145±10 meV (a value matching the trans-gauche isomerization energy, E_{TG} = 138 meV) to very small values, as the reverse bias voltage is increased (**Fig. 6b**). For the intermediate value V_{DC} = - 0.6 V, the apparent activation energy, 60 meV, of $\Delta\varepsilon$(B2) is similar to that found in the **Si-Acid 5** junction (52 meV) **[22]**.

In contrast, a temperature-activated mechanism with bias-independent frequency, as observed for peak C, has not been reported before. In addition, the peculiar behavior observed for peak C below 183 K, namely a T-independent frequency, reminds of mechanism "A", observed in **Si-Acid 5 [22]** and in aged *n*-alkyl **Si-C12 [12]** junctions, which has been attributed to adventitious water molecules. Similarly, peak D at very high frequency and low T was not detected in the **Si-Acid 5** junction.

A first tentative identification of relaxation mechanisms among the different potential dipolar-active configurations (all-*trans* conformation, topological defects, carboxylic acid end groups) is based on their dipolar strength. In *n*-alkanes, the conformation of three-bond segments is related with three minima on the potential energy curve for the rotation around the central CH_2-CH_2 bond axis: T, G^+, G^- (*trans*, right *gauche*, left *gauche*). The most stable all *trans* conformation of tethered $(CH_2)_n$ molecular backbones can be reached (at least locally) at low temperature, as indicated by experiments and simulations [**11, 13, 16**]. Starting from such quasi-perfect conformational order, metastable non-planar defects appear with increasing temperature.

In this context, it is tempting to attribute the observed increase of $\Delta\varepsilon$(B2) with increasing temperature and reverse bias voltage to some disorder or chain defect configurations; the temperature ($T \approx$ 150-200 K) for the appearance of gauche defects in molecular dynamics calculations coincides with the onset of peak B2 ($T_D \approx$ 175 K) although the latter value may slightly

depend on the proper choice of relaxation peak shapes. In this hypothesis, T_D represents a transition temperature between the low-temperature ordered phase of the OML and the high-*T* phase with gradually increasing topological disorder. Conversely, the constant value of $\Delta\varepsilon$(B1) for $T \leq 233$ K indicates that mechanism B1 must be attributed to a non-defective configuration, e.g. reorientation of a carboxylic acid dipole or TTTTT → TG^+TG^-T kink creation.

4.2 Dynamics of gauche defects in tethered *n*-alkane OML

It is usually considered that defects that are not energetically too costly will exist in equilibrium proportions determined by their Boltzmann factor, $\exp(-E_D/kT)$. However, despite low energy difference (ΔE = 20.9 meV) and small isomerization barrier (E_{TG} = 138 meV) between a stable all *trans* conformation and a metastable *gauche* defect in short alkane molecules [**37, 38**], the occurrence of isolated *gauche* bonds can be ruled out in *n*-alkyl monolayers with a moderately high coverage (typically 0.30-0.45 nm^2 footprint as compared with 0.18 nm^2 in bulk polyethylene) because the area occupied by one molecule would change significantly with the position of the *gauche* bond along the chain. In contrast, formation of a "kink" in an otherwise all *trans* chain (e.g. $TTTG^+TG^-TTT$) causes a small reduction of the end-to-end distance and leaves the planar all *trans* portions parallel to each other, but non coplanar **[18, 36, 39].** Supporting this hypothesis, simulations of anchored bilayers indicate that, if not all *trans*, an alkane chain is expected to hold two *gauche* defects and that most of *gauche* defects are organized in pairs **[36].**

As far as chain dynamics in dense tethered OML is concerned, transitions must take place in relatively short chain segments causing a minimum disturbance in the orientation of the chain at either end of the segment **[39]** and obviously no positional change at the substrate binding site. Transition mechanisms without motion of the end stems, such as rotation of a 3-bond sequence (TGT) or 5-bond sequence (TGTGT) around the fixed stem bonds (so-called crankshaft motions), clearly appear to require too much volume **[40].** Transitions with some rotational or translational shift of molecular segments should rather be considered.

In the following, the nature of defects and relaxation mechanisms in tethered OML is discussed in relation with molecular mechanics calculations of conformational transitions **(Table 2).** In the molecular mechanics approach, the energy of a molecule that can change conformation and be distorted is described as the sum of the energies of its individual bonds (bond twisting, bending …) and the energies of steric interactions between different parts of the molecule and its neighbors. An energy landscape dependent on internal coordinates (torsional angles, bond angles, bond lengths) is calculated from parameterized force fields to find a minimum energy pathway (saddle-point) along one reaction coordinate; transition rates between restricted conformational states can be obtained from vibrational partition functions of the initial and excited (saddle point) states within Eyring's transition state theory **[41]**.

Microscopic mechanism	Calculated E_{ACT} (eV)	Ref.
Kink creation	**0.38**	**a**
TTTTT → TG^+TG^-T	**0.23**	**b**
	0.18-0.23	**c**
Kink suppression	**0.08**	**a**
TG^+TG^-T → TTTTT		
Kink inversion	**0.42**	**a**
TG^+TG^-T → TG^-TG^+T	**0.39**	**b**
Kink migration	**0.38-0.42**	**d**
$TTTG^+TG^-$ → TG^+TG^-TT	**0.57 (matrix)**	**d**
	0.20 - 0.30	**b**
Five-bond crankshaft	**0.23**	**d**

Table 2 : Molecular mechanics calculations of energy barriers, E_{ACT}, for conformational transitions in short *n*-alkyl chains: a) ref. 18, b) ref. 39, c) ref. 42, d) ref. 43.

A weak dependence of kink energetics on environmental constraints was reported in several works **[18, 39]**. The kink energy is located at about 0.32 eV above the all *trans* conformation energy, as derived from short polyethylene chains, **[18]**) and the kink annihilation transition (TG^+TG^-T → TTTTT) has a very small energy barrier (0.084 eV) **[18]**. Creation and annihilation (TTTTT ↔ TG^+TG^-T) of kink defects have been modeled in short polyethylene $(CH_2)_n$ **[18],** poly(oxyethylene) $[(CH_2)_2 –O]_n$ **[39]** and polypropylene **[42]** chains. The kink creation (TTTTT → TG^+TG^-T) barrier was estimated at 0.38 eV in $C_{14}H_{39}$ linear chains **[18]**, a value larger than twice the isomerization barrier E_{TG} (0.28 ev); in contrast, significantly smaller values (0.18-0.23 eV) were derived for linear chains containing ester bonds **[39]** or polypropylene **[42]**.

Energetics and transition barriers have also been investigated for different kink motions, e.g. kink migration ($TTG^+TG^- \leftrightarrow G^+TG^-TT$) or kink inversion ($TG^+TG^-T \leftrightarrow TG^-TG^+T$) **[39, 42, 43]**. Kink migration consists in a longitudinal motion by two CH_2 units along the polyethylene backbone which leaves the remainder of the chain conformation entirely unaffected. A wide range of kink migration barriers (0.20-0.42 eV) has been reported, depending on the degree of correlation between successive bond angle rotations (e.g. $TTG^+TG^- \rightarrow TTTTT \rightarrow G^+TG^-TT$). A large matrix effect was also reported with a typical 0.15 eV increase in the kink migration barrier **[43].**

Kink inversion (or flip-flop motion) has been proposed as the dominant mechanism for the γ relaxation at low temperature in polyethylene **[18, 40]**. By exchange of the senses of the gauche bonds ($TG^+TG^-T \leftrightarrow TG^-TG^+T$), a kink is converted into its mirror image **[40].** Kink inversion does not involve any change in the chain length but rather a translational shift of one of the chain stems (on the tail side in the case of a tethered chain) with respect to the other, which implies some interactions with the neighbor molecules. The kink inversion barrier ($TG^+TG^-T \leftrightarrow TG^-TG^+T$) was estimated at 0.42 eV in $C_{14}H_{39}$ chains **[18],** a value very similar to the kink creation barrier.

In summary, large calculated barriers above 0.5 eV only appear when strong matrix effects are explicitly included in the modeling of kink defect energetics. Several kink motion mechanisms, with barriers in the range 0.38-0.46 eV, are consistent with experimental activation energies for peaks B2 and C. This result comforts the attribution of B2 relaxation to some kink inversion or translation mechanism.

4.3 Dynamics of carboxylic acid tails in tethered *n*-alkyl OML

Since peak C was not observed in the **Si-Acid 5** junction, it should rather be attributed to the dynamics resulting from the carboxylic end groups. A similar statement can be inferred from the curvature in the Arrhenius plot of peak B1 relaxation frequency, a feature lacking in the **Si-Acid 5** junction.

Simulations indicate that two types of effects can be expected in carboxylic acid-terminated *n*-alkyl OML: a) in addition to van der Waals interactions between alkyl chains (80 meV / methylene unit **[44]**), dipolar and H-bonding interactions occur between carboxylic acid-end groups, b) the formation of H-bond networks is accompanied by a high fraction of gauche conformations in the last two dihedral angles and by bending of the alkyl chains **[14].**

Interestingly, the activation energies observed at low V_{DC} for peak B1 (0.32 and 0.71 eV) nearly coincide with the electrostatic part of the interaction energy, respectively for a single H-bond (0.26-0.32 eV) and for a gas phase dimer (0.72 eV) formed between two short carboxylic acid-terminated *n*-alkyl molecules **[44]**. In carboxylic acid-functionalized SAMs, molecular dynamics

simulations of hydrogen-bond structure and dynamics have shown that roughly half of all adjacent acid groups are involved in hydrogen bonds **[45]**; additional H-bonding interactions may also occur with physisorbed water molecules **[46]** and COOH end-groups are expected to promote the penetration of water molecules **[31]**.

In this context, the transition observed near T_H = 213 K in the behavior of B1 peak frequency, typically from $E_{LT}(B1) \approx 0.32 \pm 0.02$ eV to $E_{HT}(B1) \approx 0.70 \pm 0.05$ eV, could result from a gradual change in the preferential hydrogen-bond structure from one to two H-bonds, on average. Considering that the energetics of the global system is the sum of van der Waals interactions between tethered alkyl chains and dipolar interactions between carboxylic acid-end groups, the ordered low-temperature phase of the OML is governed by the former contribution which imposes stronger topological constraints on the formation of H-bonds, while van der Waals interactions between alkyl chains are probably weaker in the disordered high-T phase, leaving more degrees of freedom for the more demanding formation of carboxylic acid dimers. This transition coincides with a narrowing of peak B1 (n_1 = 0.20) above 213 K which reveals some relaxation between independent units (Debye-type, n_B = 0) rather than a highly collective relaxation (n_B = 1), consistent with weaker correlations between relaxing units as temperature increases.

Hydrogen bond formation between carboxylic acid-end groups and adventitious water molecules is a good candidate to explain the presence of mechanism C in the **Si-Acid 100** junction, for three reasons. First, in contrast with all other observed mechanisms, peak C shows a very small increase in the activation of relaxation frequency with applied reverse voltage, showing weak coupling of the transition strain with electrostatic stress, as explained in **Section 4.4**. Second, peak C follows a similar coupling with elementary excitations of the $(CH_2)_n$ backbone (as discussed in **Section 4.5**) which would be surprising for other mechanisms such as water-water H-bond interactions. Third, a temperature-activated mechanism with bias-independent frequency, has not been observed in the **Si-Acid 5** junction; in contrast mechanism "A", attributed to adventitious water molecules, was characterized by both bias-independent and T-independent frequency over the same temperature range **[22]**.

4.4 Interpretation of increased activation energy with bias voltage

The decrease in peak frequency values with increasing reverse bias voltage **(Fig. 5)** essentially results from the increase in activation energy of the relaxation frequency. As shown in **Fig. 8**, variable sensitivity, $W(B2) > W(B1) > W(C)$ in descending order, is found for the different mechanisms in the **Si-Acid 100** junction.

Considering the kink motion mechanism (B2), the V_{DC} dependence found in the **Si-Acid 100** junction can be expressed using a forced quadratic approximation: E_{B2} (eV) = 0.38 + 0.31

$|V_{DC}|^2$ as compared with E_{B2} (eV) = 0.32 + 0.90 $|V_{DC}|^{2.5}$ in the **Si-Acid 5** junction **[22]**. This large difference is consistent with some mechanical rigidity against compressive stress brought by the hydrogen-bond structure, both in the ordered low-temperature phase (dominated by single H-bonds) and in the disordered high-*T* phase (carboxylic acid dimers).

Two alternative points of view may explain this increased energy required for defect reorientation when electrostatic pressure is increased:

a) the interaction with surrounding molecules may increase as a result of electrostriction (global tilting of chain backbones); this suppression of some degrees of freedom of molecular segments imposes motional constraints (or a decrease of the "free volume") and increases the saddle point energy along the defect reorientation path.

b) the work performed by defect reorientation in the presence of stress (normal and shear stress arising from electrostatic pressure) adds to the no-stress energy barrier. Parameter *W* is interpreted according to Boyd's statement: "*each site or state of a defect has its own strain field; reorientation of a defect from one site to another changes the strain. When this is done in the presence of a stress imposed on the specimen, work is done*" **[47]**. Indeed, the formation of a kink from an initial all *trans* chain fragment results in a shortening of the fragment which will lead to strains in the remainder of the chain and also in the surrounding lattice **[18, 39]**. Similarly, kink inversion into its mirror image gives rise locally to a change in conformation that can be propagated through the specimen as a shear strain field **[40]**. In this picture, the amount of work performed for each mechanism must thus depend on the relative orientation of strain change and stress.

Future studies of model tethered OML systems might help to discriminate these alternative concepts.

4.5 Multi-excitation entropy model

The linear correlation between activation energy of relaxation frequency and logarithm of pre-exponential factor, observed previously in the **Si-Acid 5** junction **[22]**, is confirmed in the **Si-Acid 100** junction. Characteristic inverse slope values are quite similar for mechanisms B0 (224 K), B1 (232 K), B2 (232 K) and C (222 K). Along with the existence of an isokinetic temperature ($T_F \approx$ 243±5 K for mechanism B2), this "compensation law" is interpreted using a thermodynamic description of the dipole reorientation path strongly coupled with elementary excitations collected from a thermal bath **[48]**. This behaviour has been taken as manifestation of a strong coupling of dipolar-active mechanisms with the longitudinal acoustic mode (LAM-1, bending vibration) of the C_{12} alkyl chain **[22]**.

In this work, the characteristic wavenumber of 161 cm^{-1}, corresponding to energy value the kT^* = 20 meV), is significantly lower than both wavenumber (227±10 cm^{-1}) found in the **Si-Acid**

5 junction **[22]** and calculated longitudinal acoustic modes (LAM) of a tethered C_{12} alkyl chain **[49]**. Since the chain length is essentially the same in **Si-Acid 100** and **Si-Acid 5** junctions, the most likely explanation for this low LAM frequency value is the rigidity introduced at chain ends by the hydrogen bond network [**14, 31, 45]** formed between the carboxylic acid end groups.

5 Conclusion

This work addresses the microscopic origin of dipolar relaxation peaks observed in admittance characteristics of Hg // HOOC-$C_{10}H_{25}$ – *n* Si junctions. A collective behavior of dipole dynamics in alkyl chains tethered to Si(111) is inferred from non-Debye asymmetric relaxation peak shape and strong coupling of the dipole relaxation path with longitudinal acoustic vibrations of the *n*-alkyl monolayer.

Identification of the observed mechanisms has been discussed by comparing the activation energy of relaxation frequency, considered as the barrier along the dipole reorientation path, with molecular mechanics calculations. This approach is highly valuable although modeling of matrix effects in dense OML systems is not a simple task. Attribution of peak B2 to gauche conformations organized in pairs (kinks) is consistent with both kink migration and kink inversion barriers; it explains the vanishing dipole relaxation strength below $T_D \approx 175$ K and the strong increase in kink defect probability with applied voltage, as expected from some electrostatic stress induced on the soft molecular monolayer. The transition temperature, T_D, given by the intensity of peak B2 may be considered as the "melting point" of the low-temperature ordered phase of the OML.

Formation of some hydrogen-bond network, between carboxylic acid functionalities of the **Si-Acid 100** junction, is inferred from a comparison with a similar junction bearing a low density of acid end groups. This hydrogen-bond network likely explains the additional stiffness against external electrostatic stress, revealed by weaker sensitivity of relaxation frequencies to applied voltage (for B0, B1, B2 mechanisms) and smaller longitudinal acoustic mode wavenumber of tethered *n*-alkane OML derived in the context of a multi-excitation entropy model. Peak B1 is attributed to carboxylic acid end groups with different hydrogen bond conformations; its activation energy shows a transition near $T_H = 213$ K consistent with a low-temperature phase (possibly dominated by single H-bonds) and a high-*T* phase where preferential formation of carboxylic acid dimers could be expected. In this picture, the transition temperature, T_H, given by the dynamics of peak B1 represents a useful surface probe of carboxylic acid end-group conformations.

As far as dipolar relaxation is concerned, tethered carboxylic-acid terminated *n*-alkyl monolayers is a complex assembly with a large variety of relaxation mechanisms. It is also a very interesting system to investigate the possible interplay between van der Waals energy due to tethered

alkyl chains interactions and hydrogen-bond formation between carboxylic acid-end groups. More detailed investigations will be useful to determine the consequences of the temperature-dependent and bias voltage-dependent kink defect probability on electron transport through molecular junctions.

Acknowledgments

Bruno Fabre and Cyril Herrier (Sciences Chimiques de Rennes, CNRS, University of Rennes 1) are acknowledged for molecular grafting experiments. We also thank A.B. Fadjie-Djomkam and S. Ababou-Girard (Institut de Physique de Rennes, CNRS, University of Rennes 1) for XPS and admittance measurements.

References

[1] Schreiber F 2000 Prog. Surf. Sci. 65 151

[2] Badia A, Lennox R B and Reven L 2000 Acc. Chem. Res. 33 475

[3] Akkerman H B and de Boer B 2008 J. Phys. Condens. Matter 20 013001

[4] Salomon A, Cahen D, Lindsay S M, Tomfohr J, Engelkes V B and Frisbie C D 2003 Adv. Mat. 15 1881

[5] Vuillaume D 2008 C.R. Physique 9 78

[6] Vilan A, Yaffe O, Biller A, Salomon A, Kahn A and Cahen D 2010 Adv. Mater. 22 140

[7] Fadjie-Djomkam A B, Ababou-Girard S, Hiremath R, Herrier C, Fabre B, Solal S and Godet C 2011 J. Appl. Phys. 110 083708

[8] Selzer Y, Salomon A and Cahen D 2002 J. Phys. Chem. B 106 10432

[9] Salomon A, Shpaisman H, Seitz O, Böcking T and Cahen D 2008 J. Phys. Chem. C 112 3969

[10] Frederiksen T, Munuera C, Ocal C, Brandbyge M, Paulsson M, Sanchez-Portal D and Arnau A 2009 ACS Nano 3 2073

[11] Shpaisman H, Seitz O, Yaffe O, Roodenko K, Scheres L, Zuilhof H, Chabal Y J, Sueyoshi T, Kera S, Ueno N, Vilan A and Cahen D 2012 Chem. Sci. 3 851

[12] Fadjie-Djomkam A B, Ababou-Girard S and Godet C 2012 J. Appl. Phys. 112 113701

[13] Hautman J and Klein M L 1990 J. Chem. Phys. 93 7483

[14] Hautman J, Bareman J P, Mar W and Klein M L 1991 J. Chem. Soc. Faraday Trans. 87 2031

[15] Klatte S J and Beck T L 1993 J. Phys. Chem. 97 5727

[16] Zhang L, Wesley K and Jiang S 2001 Langmuir 17 6275

[17] Singh S, Wegmann J, Albert K and Muller K 2002 J. Phys. Chem. B 106 878

[18] Boyd R H 1975 J. Polym. Sci. Polym. Phys. 13 2345

[19] Pleutin S, Clement N, Guerin D and Vuillaume D 2010 Phys. Rev. B 82 125436

[20] Clement N, Pleutin S, Guerin D and Vuillaume D 2010 Phys. Rev. B 82 035404

[21] Godet C, Fadjie-Djomkam A B, Ababou-Girard S, Tricot S, Turban P, Li Y, Pujari S P, Scheres L, Zuilhof H and Fabre B 2014 J. Phys. Chem. C 118 6773

[22] Godet C 2015 Beilstein J. Nanotechnol. 6 583

[23] Vassilikou-Dova A and Kalogeras I M 2009 Thermal analysis of Polymers: Fundamentals and Applications, ed J D Menczel and R B Prime (Hoboken, NJ: John Wiley & sons) p 497

[24] Kremer F and Schönhals A 2002 Broadband Dielectric Spectroscopy (Berlin: Springer)

[25] Biswas S K 2007 J. Indian Inst. Sci. 87 15

[26] Knorr D B, Widjaja P, Acton O and Overney R M 2011 J. Chem. Phys. 134 104502

[27] Cheng H and Hu Y 2012 Adv. Coll. Interface Sci. 171-172 53

[28] Cordier S, Fabre B, Molard Y, Fadjie-Djomkam A B, Tournerie N, Ledevna A, Naumov N G, Moreac A, Turban P, Tricot S, Ababou-Girard S and Godet C 2010 J. Phys. Chem. C 114 18622

[29] Voicu R, Boukherroub R, Bartzoka V, Ward T, Wojtyk J T C and Wayner D D M 2004 Langmuir 20 11713

[30] Asanuma, H.; Lopinski, G. P; Yu, H. Z. Kinetic Control of the Photochemical Reactivity of Hydrogen-Terminated Silicon with Bifunctional Molecules. Langmuir 2005, 21, 5013-5018.

[31] D Faucheux A, Gouget-Laemmel A C, Henry de Villeneuve C, Boukherroub R, Ozanam F, Allongue P and Chazalviel J N 2006 Langmuir 22 153

[32] Powell C J and Jablonski A 2000 NIST Electron Inelastic-Mean-Free-Path, Database version 1.1

[33] Wallart X, Henry de Villeneuve C and Allongue P 2005 J. Am. Chem. Soc. 127 7871

[34] Dissado L A and Hill R M 1979 Nature 279 685

[35] Dissado L A and Hill R M 1983 Proc. R. Soc. London A 390 131

[36] Naik V V and Vasudevan S 2009 J. Phys. Chem. C 113 8806

[37] Klauda J B, Brooks B R, MacKerell A D, Venable R M and Pastor R W 2005 J. Phys. Chem. B 109 5300

[38] Smith G D and Jaffe R L 1996 J. Phys. Chem. 100 18718

[39] Heaton N J, Benavente R, Perez E, Bello A and Perena J M 1996 Polymer 37 3791

[40] Boyd R H 1985 Polymer 26 1123

[41] Glasstone S, Laidler K J and Eyring H 1941 The theory of molecular rate processes (New York: McGraw-Hill)

[42] Bartos J and Hlouskova Z 1988 Colloid Polym. Sci. 266 624

[43] Boyd R H and Breitling S M 1974 Macromolecules 7 855

[44] Hagler A T, Dauber P and Lifson S 1979 J. Am. Chem. Soc. 101 5131

[45] Winter N, Vieceli J and Benjamin I 2008 J. Phys. Chem. B 112 227

[46] Grimm R L, Tobias D J and Hemminger J C 2010 J. Chem. Phys. C 114 1570

[47] Boyd R H 1978 Molecular basis of transitions and relaxations (Midland Macromolecular Monographs, vol. 4) ed. D J Meier (New York: Gordon and Breach Science Publishers) p 277

[48] Yelon A, Movaghar B and Crandall R S 2006 Rep. Prog. Phys. 69 1145

[49] Levin C S, Janesko B G, Bardhan R, Scuseria G E, Hartgerink J D and Halas N J 2006 Nano Lett. 6 2617

FIGURE CAPTIONS

Figure 1 : Differential conductance (G) obtained by numerical derivation of I - V characteristics of the Hg // Acid 100 – n-Si junction.

Figure 2 Temperature dependence of the admittance of the Hg // Acid 100 – Si junction (V_{DC} = 0 V): a) imaginary electrical modulus $M''(\omega)$; b) capacitance $C(\omega)$; c) real admittance $G(\omega)$. A clear discrimination between space-charge layer and OML dipolar relaxations appears in the electrical modulus representation. A larger noise level is found at the grid frequency (50 Hz).

Figure 3 Determination of asymmetric peak shape parameters (Dissado-Hill theory, **Eqn 1**) for each dipolar relaxation mechanism. The red line is the peak sum fitted to data (open triangles):

a) T = 223 K, V_{DC} = -0.60 V (m_1 = 0.70, n_A = 0.55).

b) T = 203 K, V_{DC} = -0.60 V (m_1= 0.70, n_2 = 0.50, n_A = 0.55) ;

c) T = 203 K, V_{DC} = -1.0 V (m_1= 0.70, n_2 = 0.50, n_A = 0.50) ;

d) T = 173 K, V_{DC} = -0.20 V (n_1 = 0.40, m_A = 0.70, n_A = 0.35, m_C = 0.30, n_C = 0.60).

Figure 4 Temperature dependence of the dipolar relaxation frequencies f_X (a) and dielectric strength $\Delta\varepsilon$ (b) at small reverse voltage (V_{DC} = - 0.10 V) for peaks B0, B1, B2, C, D. The lines are Arrhenius fits to the frequency data in the range 183-223 K. A transition at T_H = 213 K is observed for peak B1 frequency.

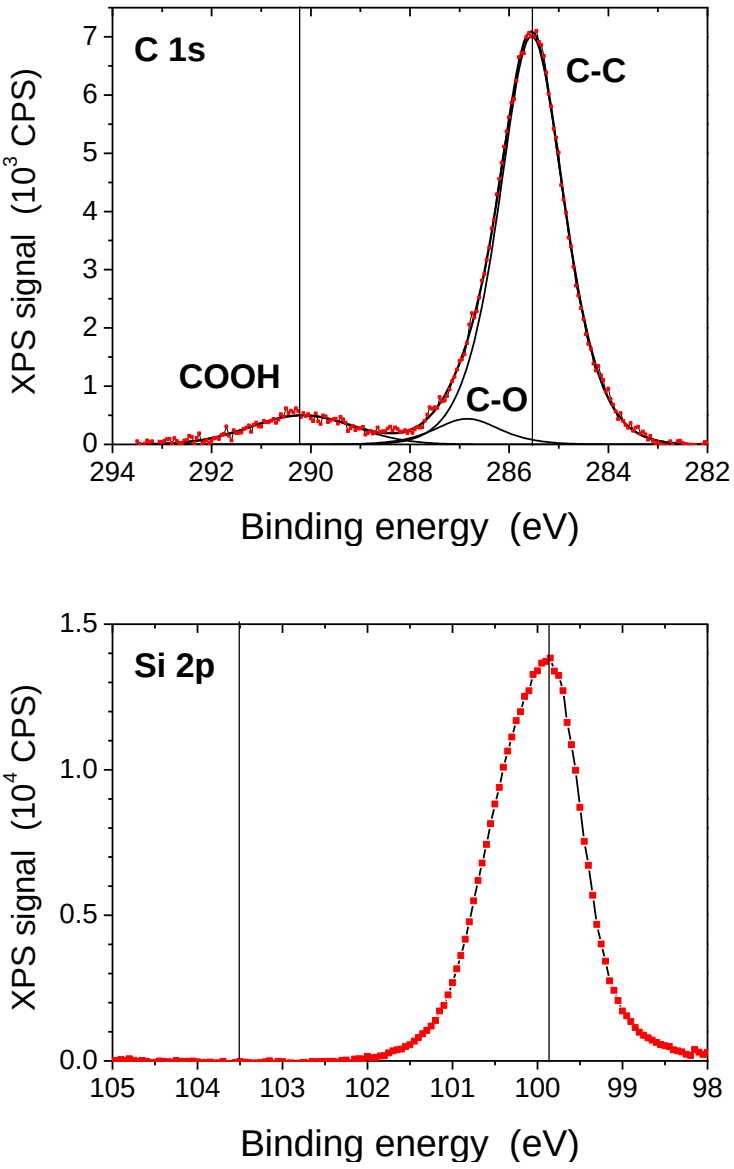
Figure 5 a) Reverse voltage dependence of relaxation frequencies for peaks B1, B2 and C at 193, 203, and 213 K. (b) Temperature dependence of f_{B2} at different reverse voltage values (V_{DC} range from -0.05 V to - 1.25 V); the lines are Arrhenius fits to the data, showing the existence of a "focal point" near T_F (B2) = 243 K.

Figure 6 Dipolar relaxation strength for mechanism B2 in the Hg // Acid 100 – n-Si junction; $\Delta\varepsilon$ (B2) increases with increasing temperature and increasing reverse voltage V_{DC} (from 0 V to - 1.0 V). The order-disorder temperature, T_D, is defined by the onset of gauche or kink defect relaxation.

Figure 7 Linear correlation between activation energy of the relaxation frequency and logarithm of pre-exponential factor derived from **Fig.4**, for peaks B0 (stars, black), B1 (LT, diamonds, red), B1 (HT, squares, red), B2 (squares, green) and C (triangles, blue). The inverse slope is denoted kT^*.

Figure 8 Activation energy of the relaxation frequency as a function of applied dc bias voltage, V_{DC}, for mechanisms B0 (stars, black), B1 (LT, diamonds, red), B1 (HT, squares, red), B2 (squares, green) and C (triangles, blue). For peak B2, the full line is a calculated power-law function with forced exponent value: E_{B2} (eV) = 0.38 + 0.29 $|V_{DC}|^2$

SUPPLEMENTARY INFORMATION



XPS spectra for the **Si-Acid 100** monolayer: a) C1s core level (α = 0°) showing C-C and COOH peaks; a very small contribution attributed to C-O bonds appears in the spectral decomposition (Shirley background, Voigt peak profiles); b) Si2p core level (α = 45°) showing that the silicon surface is oxide-free (no peak near 103.5 eV).